patient selection. Previous reports have investigated predictors of response to sclerotherapy in VM patients. For example, Berenguer et al. (1999) reported that male sex and number of sclerotherapy sessions were independent predictors of good outcomes. Goyal et al. (2002) proposed that patients with well defined, small VMs on MRI imaging had a better response to sclerotherapy. Yun et al. (2009) identified no or delayed visualization of drainage veins, a well-defined margin on MRI, and female sex as predictors of good outcomes. Mimura et al. (2009) revealed a better therapeutic effect in patients with small VMs, well-defined VMs, and VMs with good stasis of sclerosant during sclerotherapy.

In our study, adjacent bone change, maximum diameter of VM, and number of sclerotherapy sessions were significantly associated with patient satisfaction on univariate analysis. Multivariate analysis revealed that absence of adjacent bone change was an independent predictor for good satisfaction after sclerotherapy, whereas sex, VM location, VM margin, and anatomical pattern of draining veins on a venography were not. Thus, poor outcomes are expected in VMs with adjacent bone change. Mendonca et al. (2010) estimated that VMs with bone or joint involvement were associated with a higher risk of symptom recurrence. Goto et al. (2001) reported that hemangiomas with adjacent periosteal new bone formation were more painful than those without it. These results support our findings.

Bone changes adjacent to VMs (also referred to as "soft-tissue hemangiomas" in the literature) were observed in 19-63% of patients on plain film or MRI (Mendonca et al. 2010; Ly et al. 2003; Goto et al. 2001; Sung et al. 1998; Enjolras et al. 1997; Breugem et al. 2001; Pourbagher et al. 2011). In our cohort, 12 patients (30%) had bone changes adjacent to VMs. The precise mechanism of adjacent bone change remains unknown. Several factors could contribute to adjacent bone change, including physical irritation, an extrinsic pressure and passive hyperemia (Sung et al. 1998; Goto et al. 2001; Pourbagher et al. 2011). Bone homeostasis is maintained by the balance between bone resorption and formation and is affected by local oxygen tension and pH, various cytokines, and hormones (Arnett 2010). We postulate that some cytokines and the change in local oxygen tension and pH due to latent microshunts and congestion may be one of the important factors developing the adjacent bone change around VMs, but it is still no better than a conjecture.

Further investigation is needed to clarify the effect of adjacent bone change on patient symptoms that may impair patient satisfaction to sclerotherapy. Studies of local oxygen tension and pH, bone metabolic markers of osteoblast and osteoclast function, and some cytokines might be useful in this regard.

This study had several limitations. First, the study was retrospective and had a small number of patients. Further, there were no standards for treatment indication and evaluation criteria for sclerotherapy of VMs. In addition, we did not evaluate patient mental health that may affect patient satisfaction. We may take account of the use of validated quality-of-life assessment tool, such as SF-36 and the Child Health Questionnaire (CHQ).

In conclusion, percutaneous sclerotherapy was effective in relieving symptoms in patients with VMs in the extremities. Adjacent bone change was a significant predictor of patient dissatisfaction.

Author details
[1]Department of Diagnostic and Interventional Radiology, Osaka University Graduate School of Medicine, 2-2 Yamadaoka Suita, Osaka 565-0871, Japan. [2]Department of Orthopedic Surgery, Osaka University Graduate School of Medicine, 2-2 Yamadaoka Suita, Osaka 565-0871, Japan. [3]Department of Orthopedic Surgery, Osaka Medical Center for Cancer and Cardiovascular Diseases, 1-3-3 Nakmichi Higashinari, Osaka 537-8511, Japan. [4]Department of Pediatric Surgery, Osaka University Graduate School of Medicine, 2-2 Yamadaoka Suita, Osaka 565-0871, Japan.

References
Arnett TR (2010) Acidosis, hypoxia and bone. Arch Biochem Biophys 503:103–109
Berenguer B, Burrows PE, Zurakowski D, Mulliken JB (1999) Sclerotherapy of craniofacial venous malformations: complications and results. Plast Reconstr Surg 104:1–11, discussion 12–5
Blaise S, Charavin-Cocuzza M, Riom H, Brix M, Seinturier C, Diamand JM, Gachet G, Carpentier PH (2011) Treatment of low-flow vascular malformations by ultrasound-guided sclerotherapy with polidocanol foam: 24 cases and literature review. Eur J Vasc Endovasc Surg 41:412–417
Breugem CC, Maas M, van der Horst CM (2001) Magnetic resonance imaging findings of vascular malformations of the lower extremity. Plast Reconstr Surg 108:878–884
Burrows PE (2013) Endovascular treatment of slow-flow vascular malformations. Tech Vasc Interv Radiol 16:12–21
Dubois J, Garel L (1999) Imaging and therapeutic approach of hemangiomas and vascular malformations in the pediatric age group. Pediatr Radiol 29:879–893
Enjolras O, Mulliken JB (1997) Vascular tumors and vascular malformations (new issues). Adv Dermatol 13:375–423
Enjolras O, Ciabrini D, Mazoyer E, Laurian C, Herbreteau D (1997) Extensive pure venous malformations in the upper or lower limb: a review of 27 cases. J Am Acad Dermatol 36:219–225
Goto T, Kojima T, Iijima T, Yokokura S, Kawano H, Yamamoto A, Matsuda K (2001) Soft-tissue haemangioma and periosteal new bone formation on the neighbouring bone. Arch Orthop Trauma Surg 121:549–553
Goyal M, Causer PA, Armstrong D (2002) Venous vascular malformations in pediatric patients: comparison of results of alcohol sclerotherapy with proposed MR imaging classification. Radiology 223:639–644
Jin Y, Lin X, Chen LW, Hu X, Ma G, Zhu L, Sun M, Yang C, Wang W (2009) Craniofacial venous malformations: magnetic resonance imaging features that predict treatment outcome. J Oral Maxillofac Surg 67:2388–2396
Lee CH, Chen SG (2005) Direct percutaneous ethanol instillation for treatment of venous malformation in the face and neck. Br J Plast Surg 58:1073–1078
Lee KB, Kim DI, Oh SK, Do YS, Kim KH, Kim YW (2008) Incidence of soft tissue injury and neuropathy after embolo/sclerotherapy for congenital vascular malformation. J Vasc Surg 48:1286–1291

Lee BB, Baumgartner I, Berlien P, Bianchini G, Burrows P, Gloviczki P, Huang Y, Laredo J, Loose DA, Markovic J, Mattassi R, Parsi K, Rabe E, Rosenblatt M, Shortell C, Stillo F, Vaghi M, Villavicencio L, Zamboni P (2014) Guideline. Diagnosis and treatment of venous malformations. consensus document of the international union of phlebology (iup): updated-2013. Int Angiol, http://www.minervamedica.it/en/journals/international-angiology/article.php?cod=R34Y9999N00A140001. Accessed 10 Sep 2014

Ly JQ, Sanders TG, Mulloy JP, Soares GM, Beall DP, Parsons TW, Slabaugh MA (2003) Osseous change adjacent to soft-tissue hemangiomas of the extremities: correlation with lesion size and proximity to bone. AJR Am J Roentgenol 180:1695–1700

Mendonca DA, McCafferty I, Nishikawa H, Lester R (2010) Venous malformations of the limbs: the Birmingham experience, comparisons and classification in children. J Plast Reconstr Aesthet Surg 63:383–389

Mimura H, Fujiwara H, Hiraki T, Gobara H, Mukai T, Hyodo T, Iguchi T, Yasui K, Kimata Y, Kanazawa S (2009) Polidocanol sclerotherapy for painful venous malformations: evaluation of safety and efficacy in pain relief. Eur Radiol 19:2474–2480

Mulliken JB, Glowacki J (1982) Hemangiomas and vascular malformations in infants and children: a classification based on endothelial characteristics. Plast Reconstr Surg 69:412–422

Omary RA, Bettmann MA, Cardella JF, Bakal CW, Schwartzberg MS, Sacks D, Rholl KS, Meranze SG, Lewis CA (2003) Quality improvement guidelines for the reporting and archiving of interventional radiology procedures. J Vasc Interv Radiol 14(9 Pt 2):S293–S295

Pourbagher A, Pourbagher MA, Karan B, Ozkoc G (2011) MRI manifestations of soft-tissue haemangiomas and accompanying reactive bone changes. Br J Radiol 84:1100–1108

Puig S, Aref H, Chigot V, Bonin B, Brunelle F (2003) Classification of venous malformations in children and implications for sclerotherapy. Pediatr Radiol 33:99–103

Rautio R, Saarinen J, Laranne J, Salenius JP, Keski-Nisula L (2004) Endovascular treatment of venous malformations in extremities: results of sclerotherapy and the quality of life after treatment. Acta Radiol 45:397–403

Sung MS, Kang HS, Lee HG (1998) Regional bone changes in deep soft tissue hemangiomas: radiographic and MR features. Skeletal Radiol 27:205–210

Tan KT, Kirby J, Rajan DK, Hayeems E, Beecroft JR, Simons ME (2007) Percutaneous sodium tetradecyl sulfate sclerotherapy for peripheral venous vascular malformations: a single-center experience. J Vasc Interv Radiol 18:343–351

van der Linden E, Pattynama PM, Heeres BC, De Jong SC, Hop WC, Kroft LJ (2009) Long-term patient satisfaction after percutaneous treatment of peripheral vascular malformations. Radiology 251:926–932

Van der Vleuten CJ, Kater A, Wijnen MH, Schultze Kool LJ, Rovers MM (2014) Effectiveness of sclerotherapy, surgery, and laser therapy in patients with venous malformations: a systematic review. Cardiovasc Intervent Radiol 37:977–989

Yun WS, Kim YW, Lee KB, Kim DI, Park KB, Kim KH, Do YS, Lee BB (2009) Predictors of response to percutaneous ethanol sclerotherapy (PES) in patients with venous malformations: analysis of patient self-assessment and imaging. J Vasc Surg 50:589.e1–9

In Vivo Evaluation of Irinotecan-Loaded QuadraSphere Microspheres for Use in Chemoembolization of VX2 Liver Tumors

Kaishu Tanaka, MD, Noboru Maeda, MD, PhD, Keigo Osuga, MD, PhD,
Yoshiyuki Higashi, DVM, Akiyoshi Hayashi, DVM, PhD, Yumiko Hori, MD,
Kentaro Kishimoto, MD, Eiichi Morii, MD, PhD, Fumihito Ohashi, DVM, PhD,
and Noriyuki Tomiyama, MD, PhD

ABSTRACT

Purpose: To investigate the pharmacokinetics and chemoembolization efficacy of irinotecan-loaded QuadraSphere microspheres (QSMs) in a rabbit VX2 liver tumor model.

Materials and Methods: Fourteen rabbits with VX2 liver tumors were divided into two groups. In the irinotecan-loaded QSM group (n = 7), 3 mg of QSMs (30–60 μm) containing 12 mg of irinotecan (0.6 mL; 20 mg/mL) were injected into the left hepatic artery. In the control group (hepatic arterial infusion [HAI] and QSMs; n = 7), 3 mg of QSMs suspended in ioxaglic acid were injected following a bolus injection of 0.6 mL of irinotecan solution (20 mg/mL). Sequential irinotecan, SN-38, and SN-38G concentration changes were measured in plasma within 24 hours and at 1 week and in tissues at 1 week. The VX2 tumor growth rates at 1 and 2 weeks were calculated from computed tomographic images.

Results: All rabbits underwent successful embolization. Plasma irinotecan, SN-38, and SN-38G concentrations in the irinotecan-loaded QSM group showed significantly sustained release compared with the control group (P = .01). Compared with the control group, the irinotecan-loaded QSM group had significantly higher irinotecan concentration in liver tumors (P = .03) and a tendency toward higher SN-38 concentration in liver tumors (P = .29). The SN-38G tissue concentrations were below the limits of quantification. The tumor growth rate was significantly lower and the tumor necrosis rate significantly higher in the irinotecan-loaded QSM group (P = .02 and P = .01, respectively).

Conclusion: Chemoembolization via irinotecan-loaded QSMs more effectively suppresses tumor growth than chemoembolization with unloaded QSMs after HAI. A clinical feasibility study is warranted.

ABBREVIATIONS

AUC = area under the concentration–time curve, CRC = colorectal carcinoma, HAI = hepatic arterial infusion, QSM = QuadraSphere microsphere

The survival of patients with metastases of colorectal carcinoma (CRC) has been improved by recent developments in chemotherapy (1–4), whereas approximately 92% in patients treated with irinotecan-based second-line chemotherapy will experience disease progression, with a median progression-free survival interval of 3.8 months (5). Recently, clinical results of transarterial chemoembolization with the use of irinotecan-loaded embolic agents for liver metastases from CRC have been reported (6–11). Theoretically, transarterial chemoembolization with drug-eluting embolic agents is characterized by ischemia and local drug accumulation with limited systemic exposure. There are three types of embolic agents capable of loading irinotecan, QuadraSphere microspheres (QSMs; Merit Medical, South

Jordan, Utah), DC Bead (Biocompatibles, Farnham, United Kingdom), and Embozene TANDEM Microspheres (CeloNova BioSiences, San Antonio, Texas).

Although an in vitro study showed QSMs released most of the loaded irinotecan in a few minutes (12), to our knowledge, there have been no in vivo evaluations regarding the pharmacokinetic advantages of irinotecan-loaded QSMs. The purpose of the present study was to investigate the local and systemic pharmacokinetics and the efficacy of irinotecan-loaded QSMs in a rabbit VX2 liver tumor model. In addition, we compared these results with those in a control group treated with hepatic arterial infusion (HAI) of irinotecan plus QSMs.

MATERIALS AND METHODS

Animal Model

The study protocol was approved by the animal experimentation committee, and the experiments were performed in accordance with the animal care guidelines of our institution. Fourteen female New Zealand White rabbits (mean weight, 3.05 kg; range, 2.86–3.20 kg; Kitayama Labes, Nagano, Japan) were anesthetized by intramuscular injection of 0.2 mg/kg medetomidine hydrochloride (Dorbene; Kyoritsuseiyaku, Tokyo, Japan), 10 mg/kg ketamine hydrochloride (Ketalar; Diichi Sankyo, Tokyo, Japan), and 0.5 mg/kg butorphanol tartrate (Vetorphale; Meiji Seika Pharma, Tokyo, Japan). A small midline incision was made, and the left liver lobe was exposed. The VX2 tumors were cut into 1-mm^3 cubes, and three pieces were inserted into one site in each left liver lobe. The abdominal wall was sutured in two layers. The rabbits were studied 2 weeks after tumor implantation.

Preparation of Chemotherapeutic and Embolic Agents

Irinotecan solution (20 mg/mL; Nihon Kayaku, Tokyo, Japan) was loaded into QSMs 2 hours before injection. The size of the QSMs was 30–60 μm in the dry state, and the microsphere diameter was increased by a factor of approximately 2.6 times (78–156 μm) by the loading of irinotecan solution (13). For the control group, 30–60-μm QSMs were swollen to two times their original size in 320 mgI/mL ioxaglic acid (Hexabrix; Terumo, Tokyo, Japan) (14,15), and the diameter of QSMs was similar in both groups.

Tumor Treatment Procedure

The femoral artery was surgically exposed, and a 4-F sheath (SuperSheath; Medikit, Tokyo, Japan) was inserted. Under fluoroscopic guidance, a 4-F catheter (Selecon PA catheter, Berenstein type; Terumo Clinical Supply, Gifu, Japan) was inserted into the celiac axis, and a 1.8-F microcatheter (Pixie; Tokai Medical Products, Aichi, Japan) was advanced coaxially into the left

hepatic artery. We referred to the arterial anatomy described by Seo et al (16). Chemoembolization and intra-arterial chemoinfusion/embolization were performed in approximately 6 minutes. Irinotecan-loaded QSMs were invisible under radiographic fluoroscopy because they were flushed with distilled water to prevent elution of irinotecan from irinotecan-loaded QSMs in a syringe and a microcatheter during injection. Therefore, chemoembolization was performed without fluoroscopic guidance (13).

Study Design and Treatment Groups

In each rabbit, 3 mg of QSMs and 12 mg of irinotecan in solution were injected into the left hepatic artery. Fourteen rabbits were randomly divided into two groups. Rabbits in the irinotecan-loaded QSM group (n = 7), received 3 mg of QSMs containing 12 mg of irinotecan in solution, and rabbits in the control group (ie, HAI and QSMs; n = 7), received 3 mg of QSMs (30–60 μm in diameter) suspended in 0.6 mL of ioxaglic acid (320 mgI/mL) immediately after bolus injection of an equivalent amount of irinotecan solution. Twelve rabbits were euthanized at 7 days, and the following five variables were determined: (i) irinotecan, SN-38 (active metabolite of irinotecan), and SN-38G (inactive metabolite of SN-38) concentrations in plasma; (ii) irinotecan, SN-38, and SN-38G concentration in local tissues; (iii) growth rate of the VX2 tumor; (iv) serum chemistry; and (v) histopathologic variables. One rabbit in each group (n = 2) was euthanized at 14 days, and the growth rates of the VX2 tumor were calculated.

Pharmacokinetic Analysis

Blood samples (3 mL) were collected at 5, 10, 30, and 60 minutes and at 1 and 7 days. Another 1-mL blood sample was collected just before the procedures and at 1 and 7 days to determine the serum levels of aspartate aminotransferase, alanine aminotransferase, albumin, total bilirubin, lactase dehydrogenase, alkaline phosphatase, and γ-glutamyl transpeptidase.

The entire liver was excised and carefully removed. Samples (approximately 5-mm^3 cubes) of liver tumors, liver parenchyma adjacent to the tumor, and liver parenchyma at least 1 cm apart from the tumor were obtained for determination of tissue irinotecan, SN-38, and SN-38G concentration. The plasma or tissue concentration was determined by using high-performance liquid chromatography (Alliance HPLC; Nihon Waters, Tokyo, Japan).

For pathologic evaluation, the liver samples (5-mm^3 cubes) were embedded in paraffin. The paraffin blocks were cut at nominal 4-μm intervals and stained with hematoxylin and eosin. The tumor necrosis rate was estimated by visual inspection by using a whole-slide imaging device (NanoZoomer 2.0-HT; Hamamatsu Photonics, Shizuoka, Japan).

Imaging Analysis

The volume of the VX2 tumor was evaluated before treatment and at 7 and 14 days after treatment with computed tomography (CT; Aquilion One; Toshiba Medical Systems, Tochigi, Japan). Scanning parameters included helical acquisition, a 0.5-mm section thickness, 80 kVp, 120 mA, and a 180-mm field of view. Iohexol (6 mL; Omnipaque; Daiichi Sankyo, Tokyo Japan) was intravenously injected, and helical acquisition was initiated at 60 seconds. The tumor volume was measured by using CT volumetry (AW server 2; GE Healthcare Japan, Tokyo, Japan). The growth rate of the tumor was calculated as follows:

[(Tumor volume after treatment– Tumor

volume just before treatment)/Tumor

volume just before treatment] × 100

Statistical Analysis

The plasma irinotecan, SN-38, and SN-38G concentrations and the serum chemistry data were compared between the two groups by repeated-measures analysis of variance. The analysis of area under the concentration–time curve (AUC) was conducted by using a noncompartmental method with the trapezoidal rule (model, plasma date, bolus intravenous administration; WinNonlin professional version 6.3; Pharsight, Mountain View, California) and compared between the two groups by Mann–Whitney test. The tissue concentration, VX2 tumor growth rate, and tumor necrosis rate were compared between the two groups by Mann–Whitney test. The correlation between the growth rate of the VX2 tumor and the tumor necrosis rate was evaluated by Spearman correlation coefficient by rank test. A P value lower than .05 was considered statistically significant. All statistical analyses were conducted by using Statcel statistical software (version 3; OMS Publishing, Saitama, Japan).

RESULTS

Pharmacokinetic Analysis of Blood Samples

In both groups, the mean plasma concentrations of irinotecan peaked in 30–60 minutes, and the mean plasma concentrations of SN-38 and SN-38G peaked within 30 minutes. Plasma irinotecan, SN-38, and SN-38G concentrations in the irinotecan-loaded QSM group showed significantly sustained release compared with the HAI plus QSM control group ($P = .01$; Fig 1).

The AUC from time zero to infinity for irinotecan was significantly lower in the irinotecan-loaded QSM group than in the HAI plus QSMs group (26,616 h·ng/mL ± 5,606 vs 36,483 h·ng/mL ± 7,837; $P = .03$). The between-group differences in AUC from time zero to infinity for SN-38 (173 h·ng/mL ± 73 vs 193 h·ng/mL

± 115; $P = .74$) and SN-38G (516 h·ng/mL ± 256 vs 1,067 h·ng/mL ± 702; $P = .14$) were not significant.

Pharmacokinetic Analysis of Tissue Samples

In the irinotecan-loaded QSM group, the mean tissue irinotecan concentrations were 32.17 ng/g, 7.62 ng/g, and 9.97 ng/g in liver tumors, liver parenchyma adjacent to the tumor, and liver parenchyma at least 1 cm apart from the tumor, respectively. In the HAI plus QSM group, the mean tissue irinotecan concentrations were not calculated because they were below quantifiable limits (< 4 ng/g) in more than half of the animals. The tissue concentrations of irinotecan in liver tumor were significantly higher in the irinotecan-loaded QSM group ($P = .03$).

The tissue SN-38 concentrations in liver tumor and liver parenchyma adjacent to the tumor were higher in the irinotecan-loaded QSM group (463.33 ng/g and 4.11 ng/g, respectively) than in the HAI plus QSM control group (64.30 ng/g and below quantifiable limits, respectively), but the difference was not significant ($P = .29$ and $P = .20$, respectively). The concentrations in liver parenchyma at least 1 cm apart from the tumor and of SN-38G in all tissues were below quantifiable limits in both groups (Fig 2).

Serum Chemistry

There was no statistically significant difference in any parameter at any time point between the two groups ($P > .05$). In both groups, the aspartate aminotransferase, alanine aminotransferase, lactase dehydrogenase, alkaline phosphatase, and γ-glutamyl transpeptidase levels peaked at 1 day after treatment, and the peak values were higher in the irinotecan-loaded QSM group, without a significant difference ($P > .05$). Albumin and total bilirubin levels remained unchanged after treatment (Fig E1, available online at www.jvir.org).

Histologic Analysis

Histopathologic study revealed a significant difference in mean percentage of tumor necrosis between the irinotecan-loaded QSM group (63% ± 31) and the HAI plus QSM group (10 ± 18%; $P = .01$). Coagulative necrosis in the nontumorous liver parenchyma adjacent to the tumor was observed only in the irinotecan-loaded QSM group (n = 3; Fig 3).

Imaging Analysis

There was no significant between difference in pretreatment tumor volume ($P = .82$). The mean growth rate of the tumor was significantly lower in the irinotecan-loaded QSM group (76% ± 88) than in the HAI plus QSM group (492% ± 541; $P = .02$; Fig 4).

The tumor growth rates at 14 days were 227% in the irinotecan-loaded QSM group (379 mm^3 before treatment,
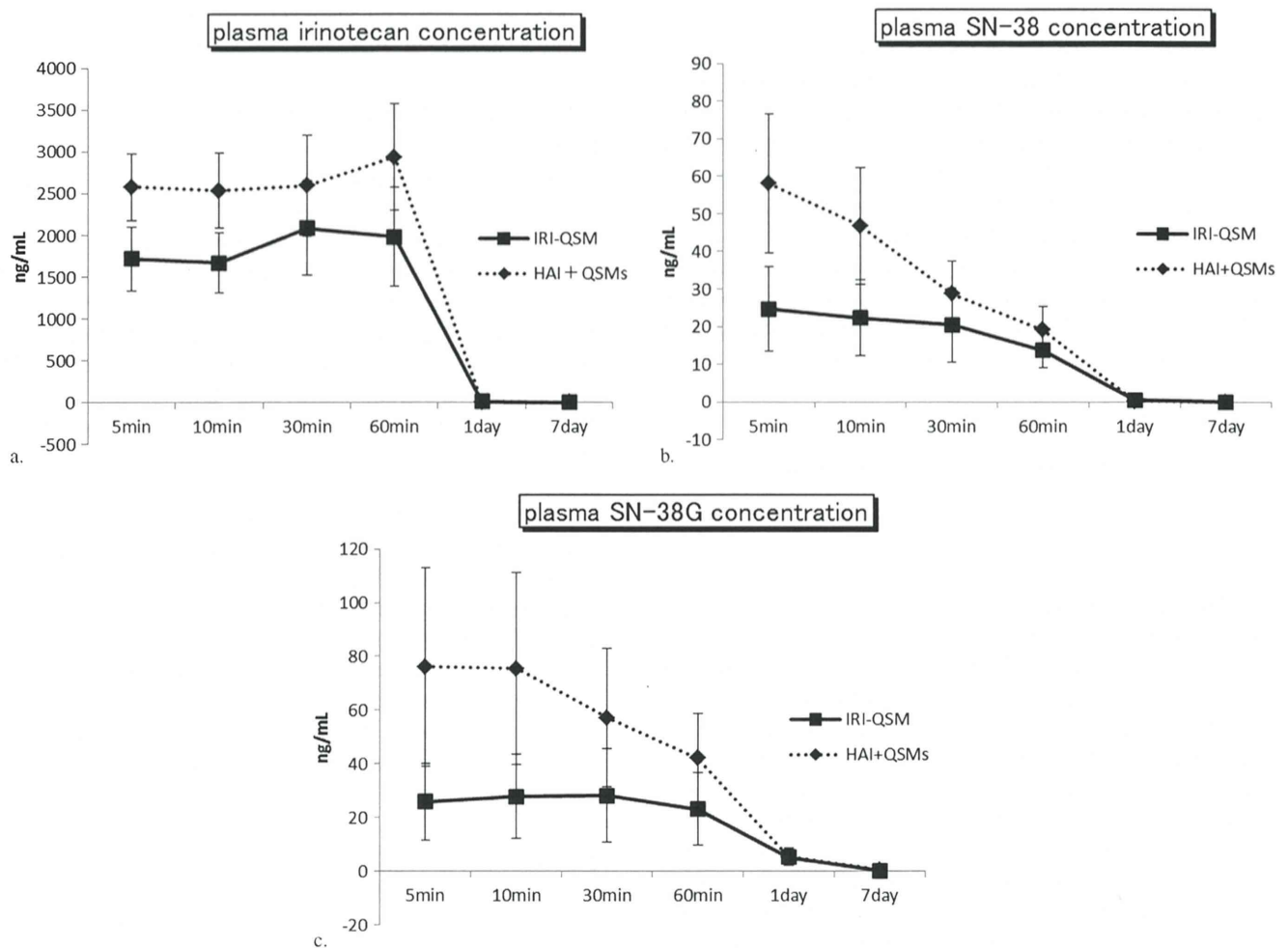
Figure 1. Pharmacokinetics of plasma irinotecan (a), SN-38 (b), and SN-38G (c) concentrations. Plasma irinotecan, SN-38, and SN-38G concentrations in the irinotecan-loaded QSM group showed significantly sustained release compared with the HAI plus QSM group ($P = .01$).

968 mm³ at 7 d, and 1,240 mm³ at 14 d; Fig 5) and 640% in the HAI plus QSM group (558 mm³ before treatment, 1,820 mm³ at 7 d, and 4,130 mm³ at 14 d; Fig 6). Histopathologic analysis showed that growth rate was significantly correlated with tumor necrosis rate (Spearman correlation coefficient −0.776; $P = .01$).

DISCUSSION

Irinotecan is a key drug for CRC and is converted to SN-38, which is 1,000-fold more cytotoxic than irinotecan, by carboxylesterase. Otherwise, SN-38 induces severe side effects, including myelosuppression and diarrhea (17,18). Therefore, transarterial chemoembolization with irinotecan-loaded embolic agents has been expected to reduce systemic toxicity and maximize the antitumor effect in the treatment of liver metastases from CRC. Several studies have reported low systemic toxicity and encouraging antitumor effects of chemoembolization with irinotecan-loaded embolic agents (7–10).

Recently, a clinical phase III study reported by Fiorentini et al (11) showed longer overall survival

(7 mo) and progression-free survival (3 mo) in a chemoembolization group treated with irinotecan-loaded DC Bead compared with a control group that received systemic chemotherapy for liver metastases from CRC. Huppert et al (6) reported the first clinical results of chemoembolization with the use of irinotecan-loaded QSMs in patients in whom previous systemic chemotherapy had failed. The median overall and progression-free survival intervals after the first chemoembolization were 8 months and 5 months, respectively, and the median overall survival was longer in patients with limited intrahepatic disease (< 25%). The results of these studies are difficult to compare simply because of differences in the patient backgrounds such as the existence of extrahepatic metastases, the percentage of tumor burden, and the administered dose of irinotecan.

In an in vitro study, Jordan et al (12) reported the loading capabilities, release capabilities, and physical properties of two drug-eluting embolic agents with irinotecan (QSMs and DC Bead). They concluded that loading of both agents was sufficient (> 90%) and that the diameters of irinotecan-loaded QSMs and irinotecan-loaded DC Bead microspheres shrank by 22% and 33%,
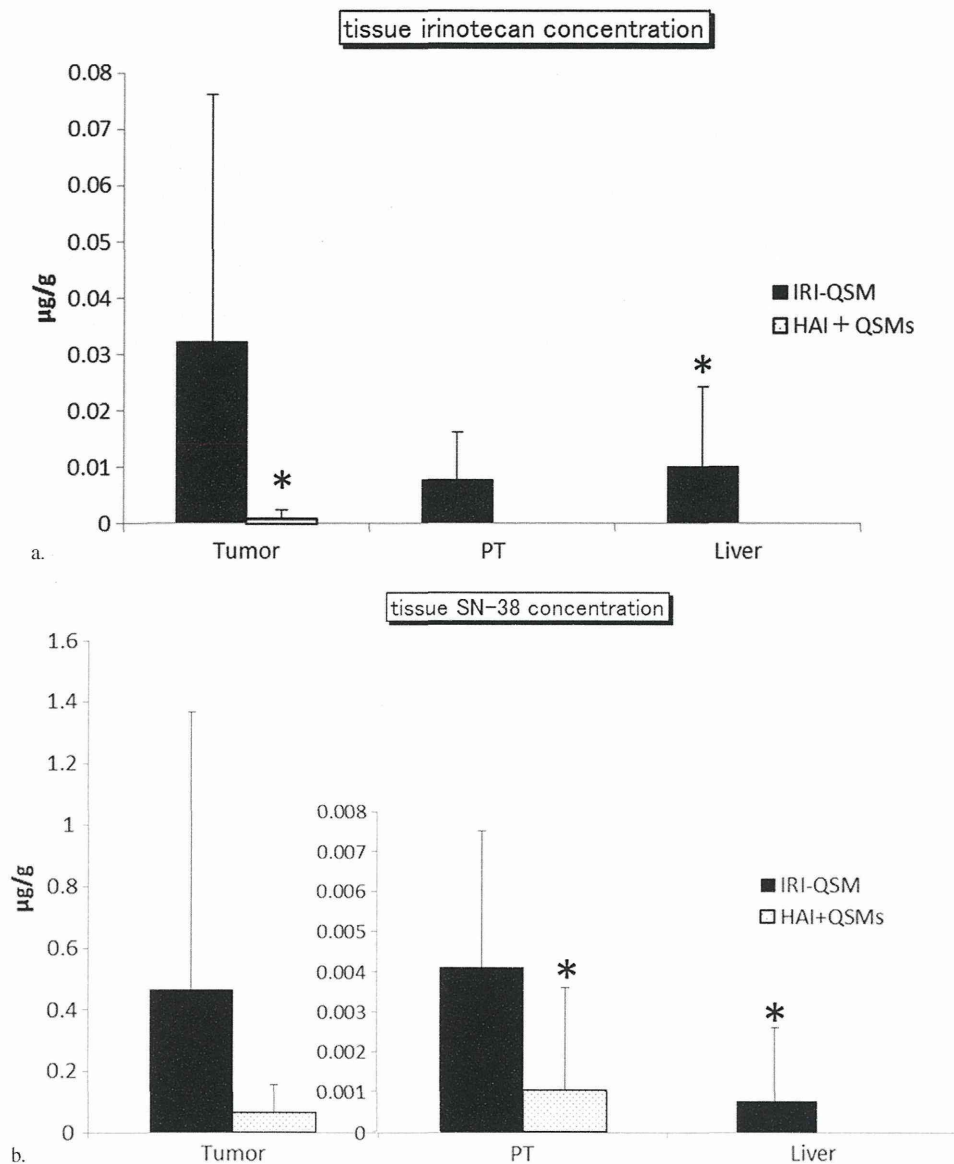
Figure 2. Tissue concentrations of irinotecan **(a)** and SN-38 **(b)** at 7 days after the start of treatment. The tissue concentration of irinotecan in the liver tumor was significantly higher in the irinotecan-loaded QSM group ($P = .03$). The tissue SN-38 concentrations in liver tumor and liver parenchyma adjacent to the tumor were higher in the irinotecan-loaded QSM group than in the HAI plus QSM group, but the difference was not significant ($P = .29$ and $P = .20$, respectively). The asterisks indicate that the data were derived only from the subjects in whom the tissue concentrations reached the quantifiable limits.

respectively, compared with the diameter of 0.9% saline solution–loaded drug-eluting embolic agents. The pattern of release and elastic properties were different. QSMs released irinotecan more quickly (in a few minutes) and were softer than DC Bead microspheres (2.9 kPa ± 0.7 vs 7.3 kPa ± 1.2).

In an in vivo study, Rao et al (19) investigated pharmacokinetics of irinotecan-loaded DC Bead. They concluded that chemoembolization with irinotecan-loaded DC Bead showed lower systemic levels of irinotecan, a high and prolonged intratumor accumulation, and a greater antitumor effect compared with intravenous/intraarterial injection. Tanaka et al (20) reported pharmacokinetics of 40-μm irinotecan-loaded

Embozene TANDEM Microspheres and concluded that they released irinotecan slowly with high drug accumulation in tumor. Serum irinotecan concentration reached a peak at 180 minutes, and tumor concentrations of irinotecan and SN-38 reached a peak at 24 hours and were detected at therapeutic levels at 72 hours, even though the amount of irinotecan was low, at approximately 3.3 mg.

The in vivo pharmacokinetics of irinotecan-loaded QSMs have not been previously investigated to our knowledge. Our focus in the present study was on irinotecan pharmacokinetics and changes in histologic characteristics after injection of irinotecan-loaded QSMs. We found that time-dependent change in plasma
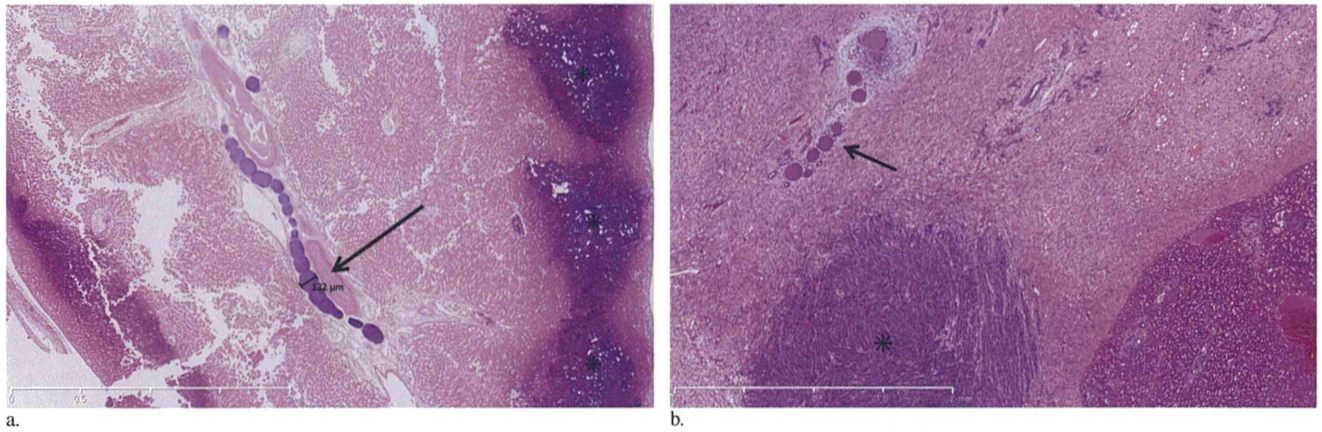
Figure 3. Pathologic images were obtained at 7 days after the start of treatment. In the irinotecan-loaded QSM group **(a)**, complete tumor cell necrosis (asterisk), and coagulative necrosis of the adjacent nontumorous liver parenchyma were observed. (Hematoxylin and eosin stain; original magnification, ×2.5.) In the HAI plus QSM group **(b)**, most of the tumor remained viable near the embolized area (asterisk). Microspheres are seen inside the arteries (arrows). (Hematoxylin and eosin stain; original magnification, ×2.5.)
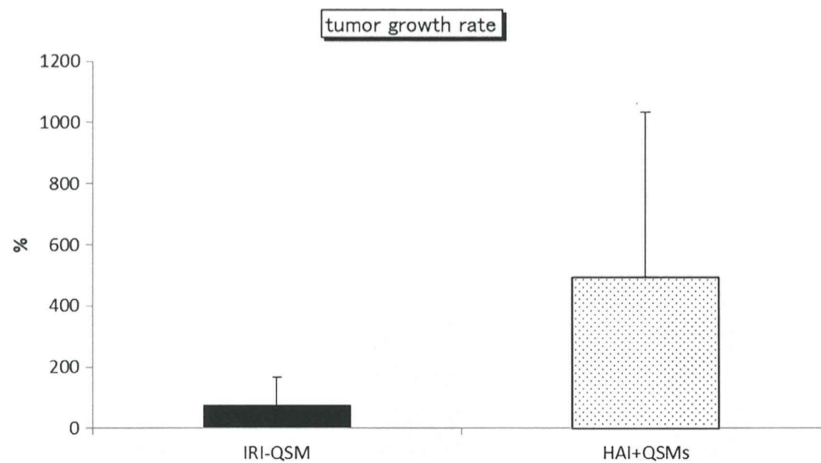

Figure 4. Tumor growth rate as a percentage. The mean tumor growth rate was significantly lower in the irinotecan-loaded QSM group ($P = .02$).

levels of irinotecan, SN-38, and SN-38G was significantly different between the two groups. Moreover, the irinotecan-loaded QSM group had a significantly lower AUC for irinotecan. Rao et al (19) reported a difference in irinotecan release from DC Bead in vivo and in vitro. The difference in irinotecan release in the present study was similar. We found that QSMs released irinotecan even at 7 days in vivo, whereas they have been shown to release irinotecan in a 7-minute burst in vitro (12). These results reflect the contribution of embolization to blood flow control and thereby to the prevention of washout of irinotecan from the embolic particles.

In both groups in the present study, accumulation of SN-38 was higher in the liver tumor than in the liver parenchyma adjacent to the tumor because uridine diphosphate glucuronosyltransferase 1A isozymes, which glucuronidate SN-38 into SN-38G during detoxification,

may be scarce in the liver tumor relative to the liver parenchyma adjacent to the tumor (21). In the irinotecan-loaded QSM group, the value of SN-38 (463.33 ng/g) in the liver tumor was approximately 10 times higher than that of irinotecan (32.17 ng/g). Tanaka et al (20) also reported higher levels of SN-38 in the liver tumor compared with those of irinotecan.

Tumor tissue levels of irinotecan were significantly higher in the irinotecan-loaded QSM group. Presumably, the significantly lower tumor growth rate and higher tumor necrosis rate in the irinotecan-loaded QSM group reflect higher intratumoral drug accumulation. Similarly, in previous reports in the VX2 liver tumor model (22,23), the pharmacokinetic profile and tumor-suppressor effect of drug-eluting embolic agents loaded with cisplatin or doxorubicin were enhanced compared with nonloaded embolic agents
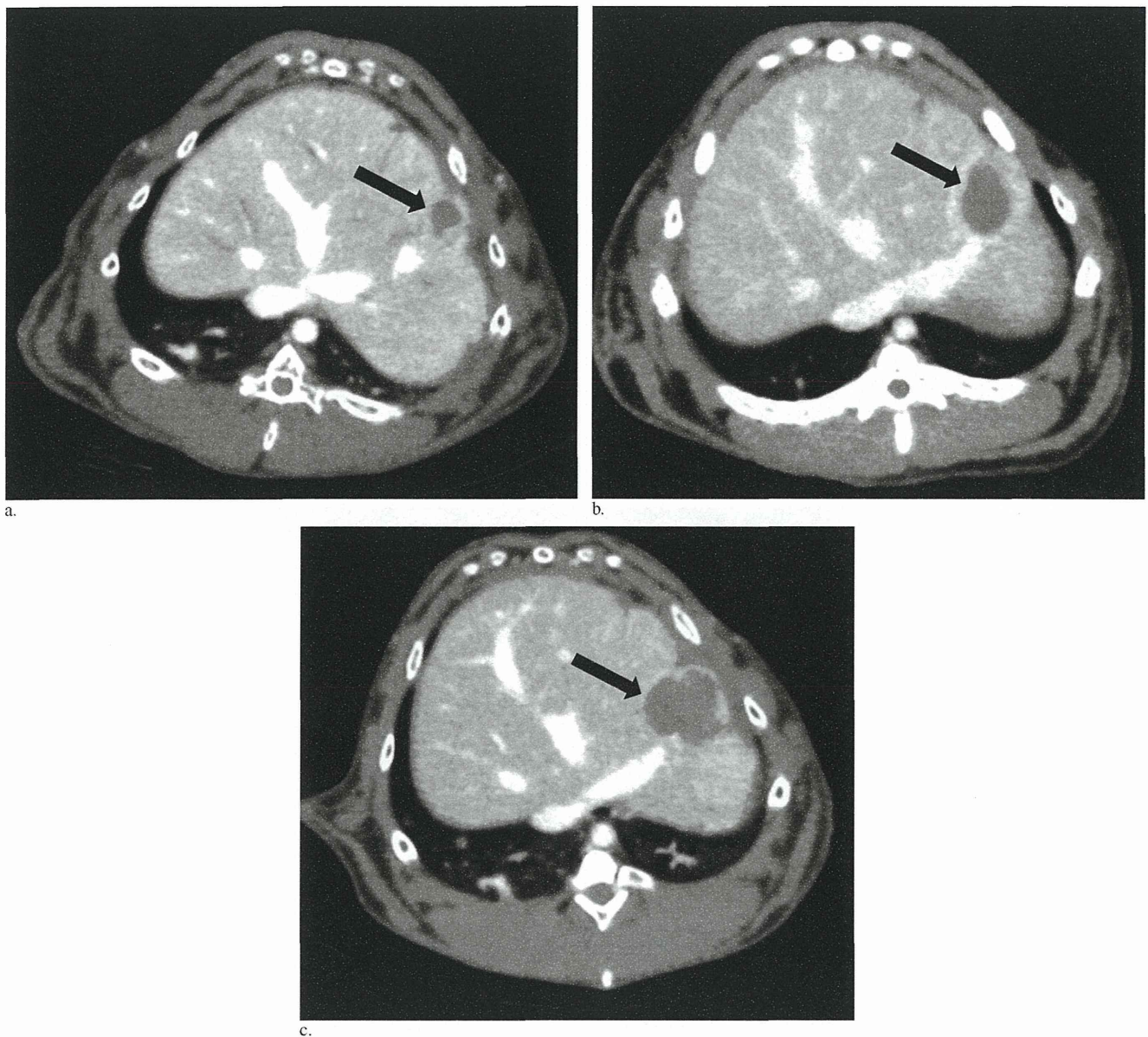
Figure 5. Contrast-enhanced CT images in the irinotecan-loaded QSM group show the tumor as a low-density mass (arrows). Before treatment **(a)**, the tumor volume was 379 mm^3. The tumor volumes increased to 968 mm^3 at 7 days **(b)** and and 1,240 mm^3 at 14 days **(c)**. The tumor growth rates over 7 days and 14 days were 227% and 370%, respectively.

after drug infusion. These results also suggest the advantage of chemoembolization via drug-eluting embolic agents.

The present study has some limitations. First, the use of a small number of rabbits led to the high variation in the results of each treatment. Second, we used rabbits implanted with VX2 liver tumors, and VX2 tumor models may not appropriately represent colorectal liver metastases, which are generally hypovascular. However, to date, no liver tumor model except for the VX2 liver model has been established for use in interventional oncology research, and the tumor has been widely used as a model for various cancers (24). Third, tumor growth rate was difficult to evaluate precisely because VX2 liver tumor tends to grow rapidly, resulting in varying degrees

of spontaneous necrosis. We measured the tumor volume based on CT findings including spontaneous necrotic areas in the tumor. Fourth, this study lacked of follow-up beyond 2 weeks, and follow-up could not be extended. However, in previous studies, QSMs were shown to release irinotecan within 7 minutes (12), and follow-up within 2 weeks was therefore considered to be appropriate. Fifth, we performed transarterial chemo-embolization without fluoroscopic guidance. In this rabbit model, the total amount of irinotecan was low, and the detection sensitivity of irinotecan may be decreased by competition for ionic binding to QSMs between irinotecan and contrast medium; ie, the elution rate of irinotecan may become higher in contrast medium (13). Moreover, QSMs may not penetrate into
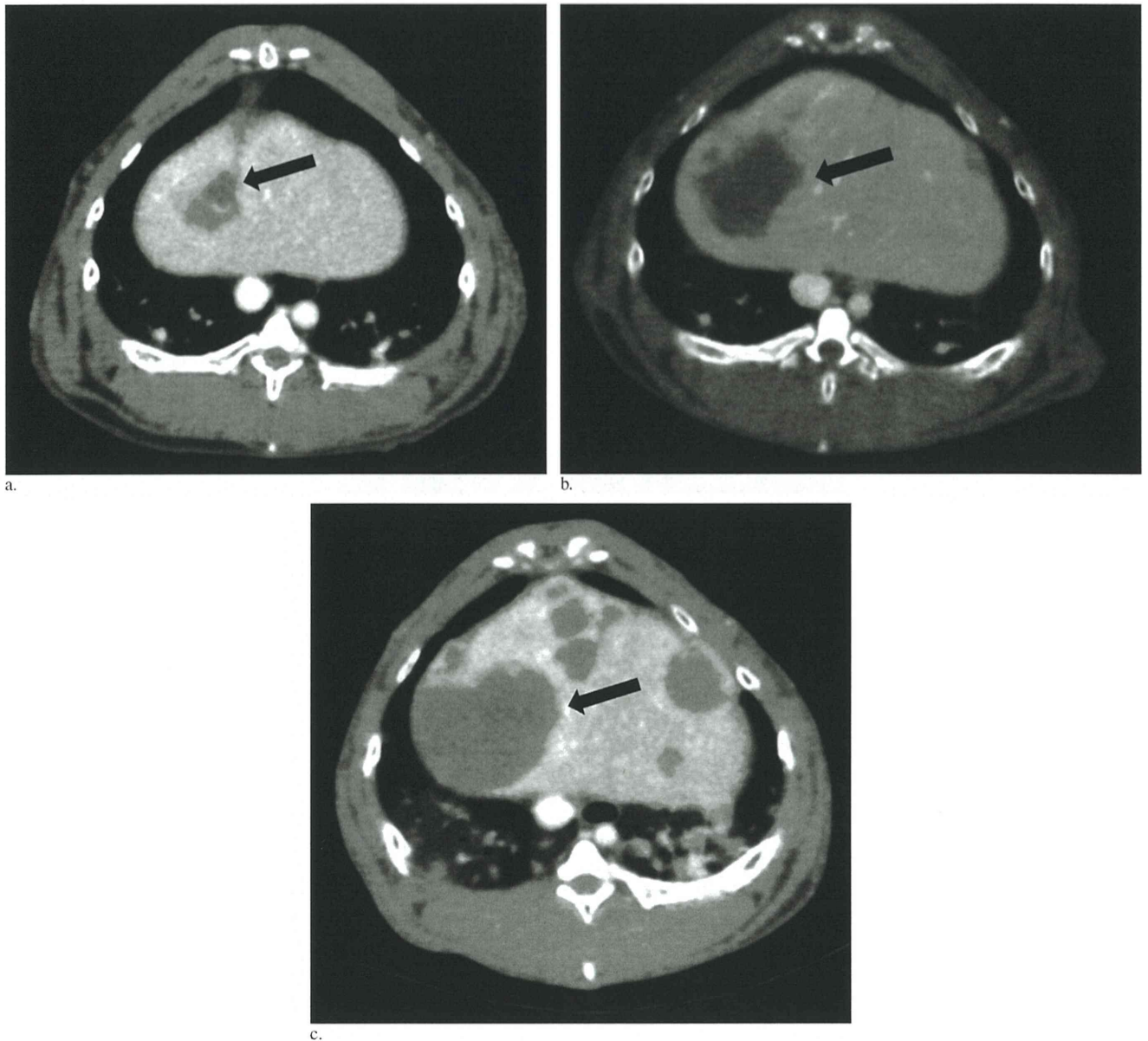
Figure 6. Contrast-enhanced CT images in the HAI plus QSM group. Before treatment **(a)**, the tumor volume was 558 mm^3. The main tumor (arrows) increased in size to 1,820 mm^3 at 7 days **(b)** and 4,130 mm^3 at 14 days **(c)**. Moreover, multiple intrahepatic metastases developed. The tumor growth rates of the main tumor over 7 days and 14 days were 226% and 640%, respectively.

tumor vessel, as QSMs in nonionic contrast media were shown to expand by approximately three to five times in an in vitro study (15). Irinotecan-loaded QSMs mixed with contrast medium should be used in clinical practice, as the elution of irinotecan in contrast media may be unlikely to have a significant impact on therapeutic effect because the amount of irinotecan is so high, at approximately 100 mg per session (7,9–11,25). In addition, de Luis et al (14) reported that the contrast medium (ionic vs nonionic) dose not affect the final size of QSMs in vivo, so QSMs in nonionic contrast media may penetrate into tumor vessel.

In conclusion, the results of the present study suggest that chemoembolization with the use of irinotecan-loaded QSMs showed sustained release of irinotecan with high accumulation of irinotecan in liver tumor, and was more effective than chemoembolization with non-loaded QSMs after HAI of irinotecan.

ACKNOWLEDGMENTS